Composites: Part A 43 (2012) 2107–2119

Contents lists available at SciVerse ScienceDirect

Composites: Part A

journal homepage: www.elsevier.com/locate/compositesa

Rheometry of compression moulded fibre-reinforced polymer composites: Rheology, compressibility, and friction forces with mould surfaces

O. Guiraud [a,b], P.J.J. Dumont [b,*], L. Orgéas [a], D. Favier [a]

[a] CNRS/Université de Grenoble (Grenoble INP – UJF), Laboratoire Sols-Solides-Structures-Risques (3SR Lab), BP 53, 38041 Grenoble cedex 9, France
[b] CNRS/Institut Polytechnique de Grenoble (Grenoble INP), Laboratoire de Génie des Procédés Papetiers (LGP2), 461 rue de la Papeterie, BP 65, 38402 Saint-Martin-d'Hères cedex, France

ARTICLE INFO

Article history:
Received 18 December 2011
Received in revised form 10 May 2012
Accepted 7 June 2012
Available online 16 June 2012

Keywords:
A. Polymer-matrix composites (PMCs)
E. Compression moulding
Rheology
C. Analytical modelling

ABSTRACT

Compression moulded preimpregnated polymer-matrix composites are often porous materials. Rheological studies usually neglect their subsequent compressible complex flow behaviour, together with mould-composite friction effects. Therefore the proposed method, including a newly developed compression rheometer, allows the rheology and the compressibility of such materials together with the mould–composite friction phenomena to be characterised without taking into account *a priori* assumptions on both the rheology of the composite and the form of the friction law. Its validity and usefulness for improving the interpretation of rheological results is demonstrated using a modelling plastic paste and an industrial Sheet Moulding Compound (SMC) during lubricated (or not) compression tests performed at low or high temperatures.

1. Introduction

Owing to their relatively high volume fraction of fibres typically ranging from 0.05 to 0.6, Sheet Moulding Compounds (SMCs) [1], Bulk Moulding Compounds (BMCs) [2], Glass Mat Thermoplastics (GMTs) [3–5], Carbon Mat Thermoplastics (CMTs) [6] or discontinuous carbon/epoxy prepregs [7,8] are lightweight compression moulded composite materials with good specific physical and mechanical properties. The fibres contained in these materials usually display a planar orientation and have a length ranging from 10 mm to 50 mm. When forming by compression thin charges (from 2 mm to 3.5 mm) of these materials, their outer layers rich in polymer act as lubricating layers that are squeezed and sheared near the mould surfaces, whereas their core rich in fibres deforms following an extensional plug flow [9,10]. Thus, similarly to fibre-reinforced mortars [11] or food materials [12,13], simple compression tests appear as relevant methods to control and to determine the rheological parameters of compression moulded materials [14,15,17,18]. Usually, the experiments are performed so as to ensure the best lubrication conditions to promote plug flow conditions, that is to minimise friction effects at the interface between the compression rheometer platens and the composite and to subject the flowing composite to the most possible homogeneous stress–strain states [19]. This allows an easier determination of the intrinsic rheological parameters of the tested composites compared with no slip or partial squeeze flow tests [20–22,19,23,24,6], for instance. Nonetheless, the friction forces induced when shearing the lubricant layers must be sufficiently low or negligible compared with the forces needed to deform the composite. In other situations, the effect of the lubricant layers in the determination of the rheological parameters can be corrected. For that purpose, arbitrary and questionable forms of the lubricant induced friction forces are commonly used [12,27,13,28,17,11].

Furthermore, it is often assumed that the composites are incompressible during flow. This assumption, currently adopted for the experimental determination of rheological parameters or the numerical simulation of mould filling, is scarcely discussed even though it is well documented, admitted, and obvious that these materials contain pores [25,26] (see also Fig. 1).

Then, this contribution aims at developing a compression device that delivers a sufficient amount of data about the flow of the tested composites. In the case of plug flow kinematics, the method proposed to analyse the acquired data reveals (i) the rheological behaviour and (ii) the compressibility of the flowing composites, and (iii) the mould–composite interface friction law without taking account of *a priori* assumptions.

2. Materials and methods

Two materials were used to develop and to validate the new compression rheometer and its analysis method: a modelling plastic plate "Play Doh" and an industrial SMC supplied by Mixt Composites Recyclages (MCR, Plastic Omnium Group, Tournon-sur-Rhône, France). The use of the modelling plastic paste is

* Corresponding author. Tel.: +33 476826921.
E-mail address: pierre.dumont@grenoble-inp.fr (P.J.J. Dumont).

1359-835X/$ - see front matter © 2012 Elsevier Ltd. All rights reserved.
http://dx.doi.org/10.1016/j.compositesa.2012.06.006

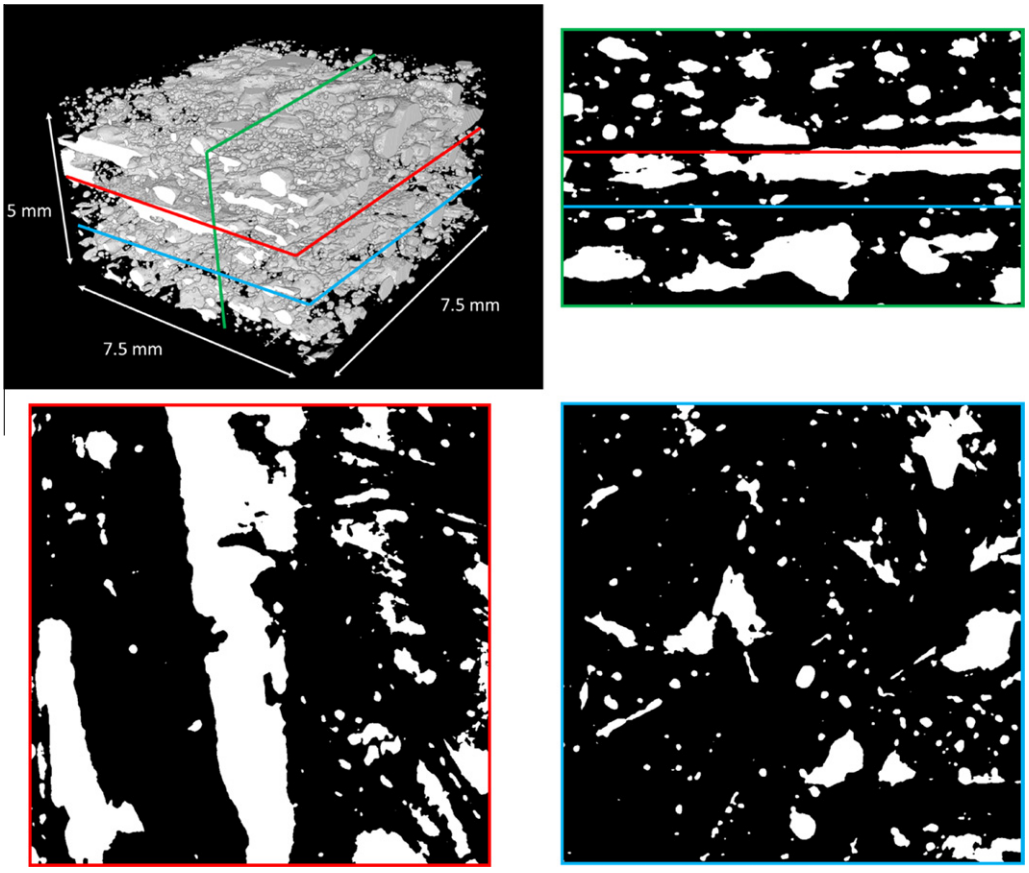

Fig. 1. Set of pictures showing a 3D view and three cross sections (pictures with coloured borders) of the porosity (in white) entrapped within a stack of four layers of SMC layers in their initial state (no curing). Image acquired using the X-ray synchrotron holotomography mode (European Synchrotron Radiation Facility (ESRF), beamline ID19, voxel size of 7.5 μm). The total porosity is here measured equal to 15%. The cross sections having the red and blue borders represent respectively the top and bottom of an individual layer of SMC within the stack. Pores of large size are particularly present in regions at the interface between several layers. The shown SMC in these images has a higher fibre content compared to that compressed, but is representative of the microstructure of the family of SMC materials. (For interpretation of the references to colour in this figure legend, the reader is referred to the web version of this article.)

interesting in view of validating the proposed system and methodology as the rheological properties of this material exhibit a limited scatter, in particular because its microstructure is rather homogeneous compared to that of SMC compounds. The SMC was reinforced with glass fibre bundles 25 mm long. Its fibre volume fraction was equal to 10.8%. It was supplied in rolls 15 m long and 0.40 m wide of thin charges where the fibres display a planar orientation. To illustrate the complex structure of SMC-like materials in their initial state before compression moulding, Fig. 1 shows a 3D representation acquired by X-ray synchrotron microtomography (European Synchrotron Radiation Facility (ESRF), beamline ID19, voxel size of 7.5 μm) of the porous phase of a stack of four SMC layers. The imaged SMC is similar to that used for compression tests, except regarding the fibre volume fraction which was higher in that case and equal to 18.8%. Both SMC were nonetheless produced on the same compounding machine, and such images are thought to be representative of the microstructure of the family of SMC materials. The initial pore content is striking. Note that such porosity value certainly corresponds to a lower bound of the porosity within SMC as, due to the scanning resolution of 7.5 μm, small pores contained, for example, within the fibre bundles or at the interface between the fibre bundles and the polymeric matrix cannot be observed. Nonetheless, despite this measurement limitation, the measured porosity value is high before moulding and the given image shows a clear example of the importance of the porosity that can be entrapped in SMC materials before compression.

Cylindrical specimens were cut in both materials. Their initial radius R_0 was equal to 55, 75 or 100 mm. For the modelling plastic paste, specimens about 16 mm in height were manually formed with a cylindrical mould. SMC specimens were composed of a stack of three SMC layers (thickness of each sample about 5 mm). All SMC specimens were cut in a central zone (10 m × 0.2 m) of the rolls to minimise possible microstructural variations. The initial thickness h_0 of the specimens was measured at the beginning of each compression test following a procedure described in the experimental sections.

Compression tests were performed using either a previously developed system [14,15] consisting of two coaxial and parallel circular plates, or the newly developed apparatus (*cf.* Section 4). These rheometers were mounted on a MTS press (maximum capacity of 20 kN and maximum cross-head velocity of 17 mm s^{-1}) where the axial strain rate could be controlled. In this study, the direction of the compression axis is given by the vector $\mathbf{e}_3$. During each test, the axial compression force F_3 was measured together with the current thickness h of the deformed sample. All tests were performed at a constant axial strain rate $|\overline{D}_{33}| = |\dot{h}/h| = 0.1\ s^{-1}$. In the case of lubricated tests, the surfaces of the platens of the compression devices were coated with a mixture of silicone grease (Molydal Al/Si 3653) and silicone oil (Julabo Thermal H5S). This mixture of lubricants was observed to ensure the best plug flow conditions for both compressed materials. Lastly, for each testing condition, experimental results were averaged over at least five tests. For isothermal test conditions, in the case of the modelling

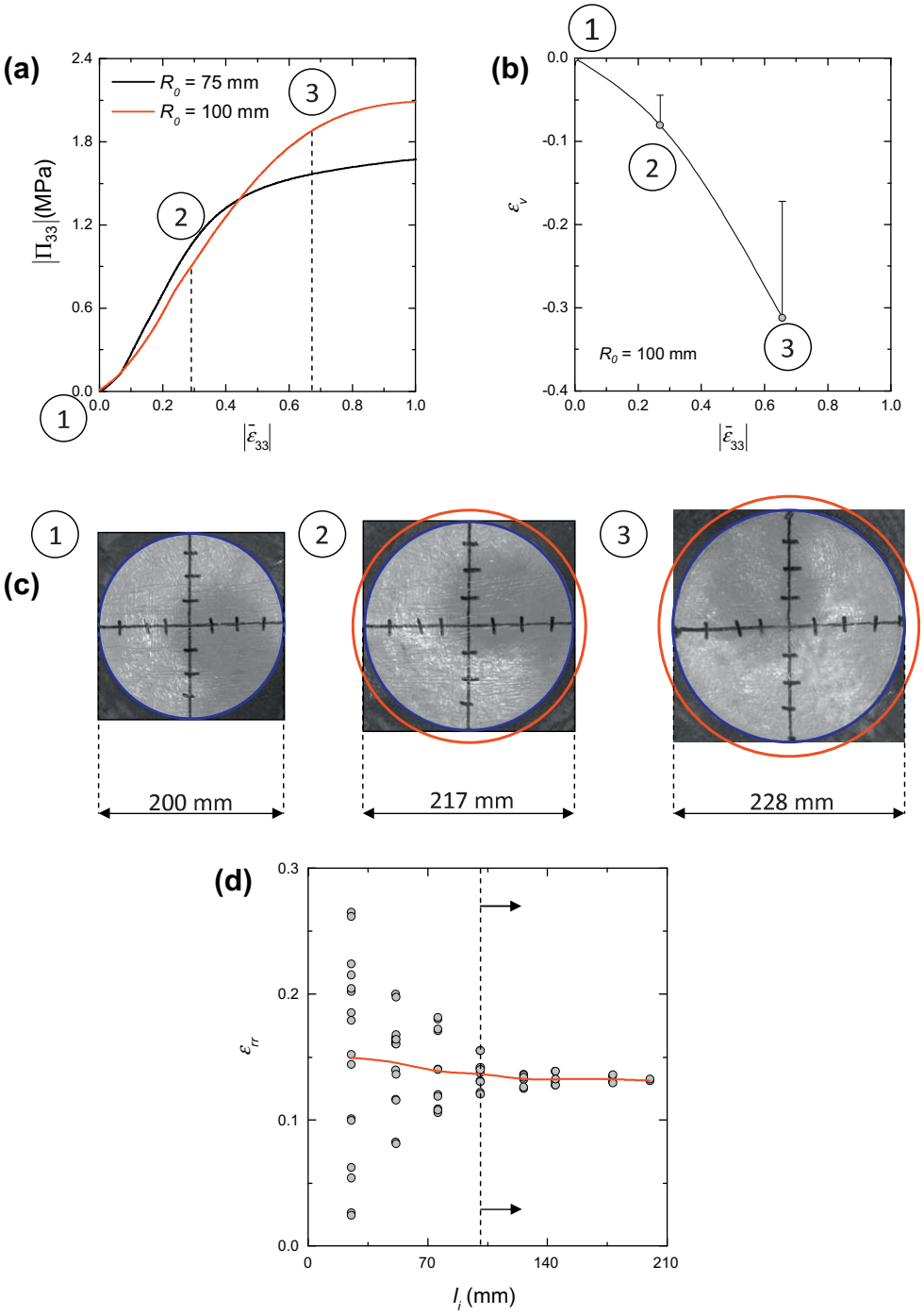

Fig. 2. Preliminary simple compression of an industrial SMC (T = 20 °C). (a) Evolution of the first Piola–Kirchhoff axial stress $|\Pi_{33}|$ as a function of the average axial strain $|\bar{\varepsilon}_{33}|$ for specimens having two different radii. (b) Evolution of the volumetric strain ε_v with respect to the average axial strain $|\bar{\varepsilon}_{33}|$. (c) Photographs of a specimen taken at various axial strains. The red circles drawn on the photographs 2 and 3 indicate the area of the specimen if this latter was incompressible. (d) Variation of the average radial strain $\bar{\varepsilon}_{rr}$ with respect to the initial length of the segment l_i considering the marks put in (c), at $|\bar{\varepsilon}_{33}| = 0.66$. Note that the apparent darkened region is simply a shadow due to the lighting system used to take the photographs. (For interpretation of the references to colour in this figure legend, the reader is referred to the web version of this article.)

plastic paste (see Sections 6 and 7) and of SMC (see Section 7), the typical scatter observed for such measurements was ±10% [16]. In the case of tests performed in anisothermal conditions, the scatter raised up to ±20% (see Section 7).

3. Preliminary experimental observations

A first series of simple compression tests was performed using the SMC, at room temperature (20 °C) and without lubrication, in order to assess the validity of several current assumptions related to the flow of short fibre composites [29,27,28,17,18]. Before each test, the specimens' wavy surfaces in contact with the mould were flattened by applying a preliminary compaction of 0.5 mm. The initial thickness h_0 of the specimens was defined after this compaction.

Fig. 2a shows the typical evolution of the average first Piola–Kirchhoff axial compression stress $\Pi_{33} = F_3/\left(\pi R_0^2\right)$ with respect to the axial strain $\bar{\varepsilon}_{33} = \ln(h/h_0)$ measured during simple compres-

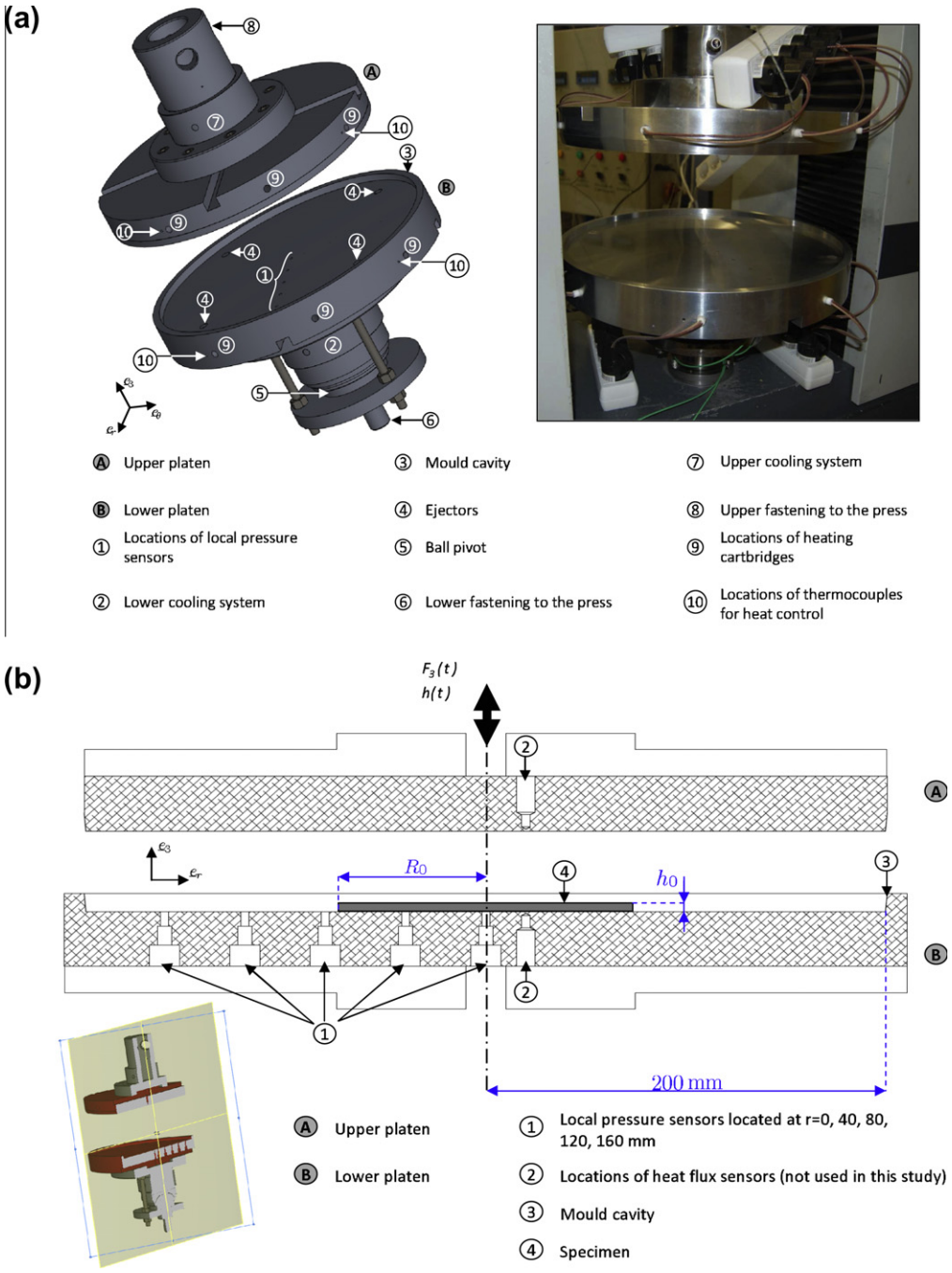

Fig. 3. (a) Schematic view and photograph of the specially designed rheometer. (b) Schematic description of the principle of simple compression tests when performed using the instrumented rheometer.

sion tests for a sample having an initial radius R_0 = 100 mm. In this figure, some photographs of the top view of one tested specimen are also given. Marks were drawn on its surface and its perimeter. These photographs were taken during an interrupted test at various deformation states, *i.e.* $\bar{\varepsilon}_{33} = 0, -0.27$ and -0.66.

3.1. Plug flow and strain homogeneity

In Fig. 2c, the assumption of a plug flow kinematics can be visually checked: the marks drawn on the perimeter of the specimen remain on it up to a large axial strain $\bar{\varepsilon}_{33} = -0.66$ during compression. Furthermore, the homogeneity of the strain was investigated using the marks drawn on the surface of the specimens, similarly to the method adopted in [15]. The average radial logarithmic strain $\bar{\varepsilon}_{rr} = \ln(l_f/l_i)$ of the specimen could be calculated by building segments of various lengths and located in various positions of the specimen's surface using the drawn marks. In this expression, l_f and l_i are the lengths of the considered segments measured before and after compression, respectively. Fig. 2d gives the variation of the radial strain $\bar{\varepsilon}_{rr}$ as a function of the initial chosen length l_i of the segments. This figure reveals that (i) the flow kinematics is highly heterogeneous for $l_i < 100$ mm showing the strong influence of the structural rearrangements occurring within the fibrous reinforcement during flow and (ii) the strain can be considered as homogeneous for segments having an initial length $l_i \geqslant 100$ mm. For this state of axial strain where $\bar{\varepsilon}_{33} = -0.66$, the average radial

strain $\bar{\varepsilon}_{rr}$ is approximately equal to 0.135. A similar strain dependence on the size of the scrutinised segments had been obtained in [15] for composites showing similar fibrous microstructures. It is clear that the size of the segments, and consequently the size of the specimen, should increase if the typical length of the fibres or fibre bundles was increased.

3.2. Compressibility of SMC

The volume V of the tested specimen was determined using the press data for the measurement of its height h and the photographs of its top surface for its in-plane dimensions in the $(\mathbf{e}_r, \mathbf{e}_\theta)$ plane. The blue circles drawn on the photographs in Fig. 2c are the real perimeters of the specimens measured by image analysis (ImageJ software), whereas the red circles depict the hypothetical perimeters of the same specimens in the case of incompressible flow. The graph shown in Fig. 2b gives the logarithmic variation of the specimen's volume $\varepsilon_v = \ln(V/V_0)$ and allows the pronounced compressibility of the tested industrial SMC to be quantified. These two results show that the specimen's volume exhibits a noteworthy decrease ranging between −20% to −30% at an axial strain $\bar{\varepsilon}_{33} = -0.66$. This phenomenon may be related to the outgassing of air or styrene entrapped within the SMC sheets or between the various sheets of the stack [25,26], see also Fig. 1b.

3.3. Evidence of friction effects at mould–composite interfaces

Fig. 2a also shows the variation of the average first Piola–Kirchhoff compression stress as a function of the average axial strain measured for specimens having two initial different radii: $R_0 = 75$ and 100 mm. It is obvious that the measured stress is much lower for the specimen with the smallest diameter, which is characteristic of friction phenomena [29,19,28,17,18,11].

4. Design of a dedicated instrumented rheometer

The simple previous examples given in the last section show that a rigorous description of the rheology of composites requires one to develop an apparatus to properly estimate the friction effects at the mould–composite interface, and the compressibility of the tested composites taking into account a minimal number of *a priori* assumptions.

To measure the friction forces, which induce gradients of the axial stress along the specimens' length and lead to an increase of the mean axial stress (see Fig. 2a), the principle of the developed rheometer is based on the no slip "squeeze" flow rheometer used in [22]; this latter was equipped with local normal axial stress sensors to determine the profile of the local axial stress during testing. In the case of simple compression tests which can be performed using lubricated (or not) conditions, the data given using these sensors has to be analysed following a specific method (*cf.* Section 5). In order to limit the cost of the developed testing apparatus, the local axial stress sensors were also used to detect the specimen in-plane flow front displacement, *i.e.* the specimen's outer, instantaneous, radius R, which gives access to a "discrete" tracking of the specimen surface. Combined with the thickness measurement, the compressibility of the composites can thus be estimated *in situ* (*i.e.* without possible springback effects). Fig. 3 shows two schemes and a photography of the instrumented developed rheometer. It is composed of two polished cylindrical platens (A) and (B) having a radius of 200 mm where the composite can flow. When closed, this mould forms a cavity (3) having a maximum thickness of 10 mm. The mould can then be completely filled with the composite during testing. Ejectors (4) are available to facilitate demoulding operations. Heating cartridges are inserted in the upper and lower platens, respectively (A) and (B), of the rheometer to perform tests at various temperatures. Each cartridge has an individual 400 W power, and is connected to a device that controls the temperature of the platens through thermocouples inserted within the mould (10). Two cooling systems are positioned above and below the upper and lower platens, respectively, to protect the load cell of the press from heating, and to ensure the thermal symmetry of the system. Five positions (1), in $r = 0$, 40, 80, 120 and 160 mm, for the local piezoelectric normal stress sensors (Kistler 6167A, 4 mm in diameter, stress range 0–20 MPa) are available along one radius of the lower compression platen (B) to measure the local axial stresses $\sigma_{33}(r)$.

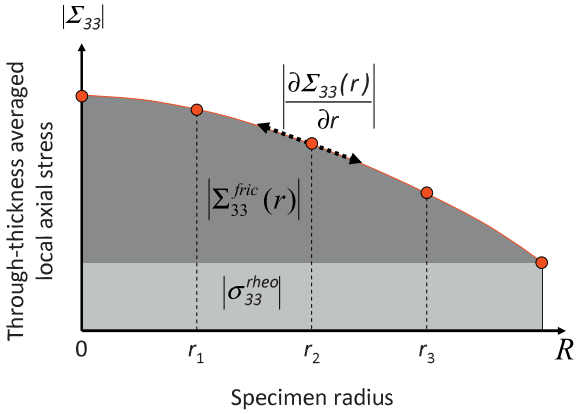

Fig. 4. Scheme showing the profile of the axial stress $|\Sigma_{33}|$ and its decomposition into its rheological and friction-induced parts encountered during a simple compression test where friction effects occur.

5. Model for the composite flow in the rheometer

In this section, a model based on the previous approaches developed for describing the flow of SMC or GMT compounds during industrial moulding operations [29,27,28] is developed to characterise with a minimal number of hypotheses (i) the rheology and the compressibility of the tested composites, and (ii) the friction forces arising at the mould–composite interface, with the help of the new rheometer presented in the previous section. For that purpose, at the macroscopic scale, the composite is assumed to be a one-phase, homogeneous and transversely isotropic, in the $(\mathbf{e}_r, \mathbf{e}_\theta)$ plane, material [29–31,15,28,32]. A homogeneous simple compression flow is assumed in the whole specimen and friction effects are considered at the interface between the upper (resp. lower) platen and the flowing composites. The possible compressibility of the composite and no *a priori* estimate for the friction forces are considered in the following flow model. These two points constitute the main originality of the proposed approach. Note that the assumption of the homogeneity of the flow is only valid at a macroscopic scale. The possible heterogeneity at a local scale of the velocity field, *e.g.* in the bulk of a multilayer compound, is averaged.

5.1. Mass balance equation

In the present model, the mass balance equation is given as follows:

$$div(\mathbf{v}) = -\frac{\dot{\rho}}{\rho} = \dot{\varepsilon}_v(t), \quad \forall\{r, x_3\}, \tag{1}$$

where $\mathbf{v}$, ρ, $\dot{\rho}$, $\dot{\varepsilon}_v$ are the velocity field, the density, the rate of change of the density, and the volumetric strain rate, respectively. It is important to note that $\dot{\varepsilon}_v$ is assumed to be spatially constant.

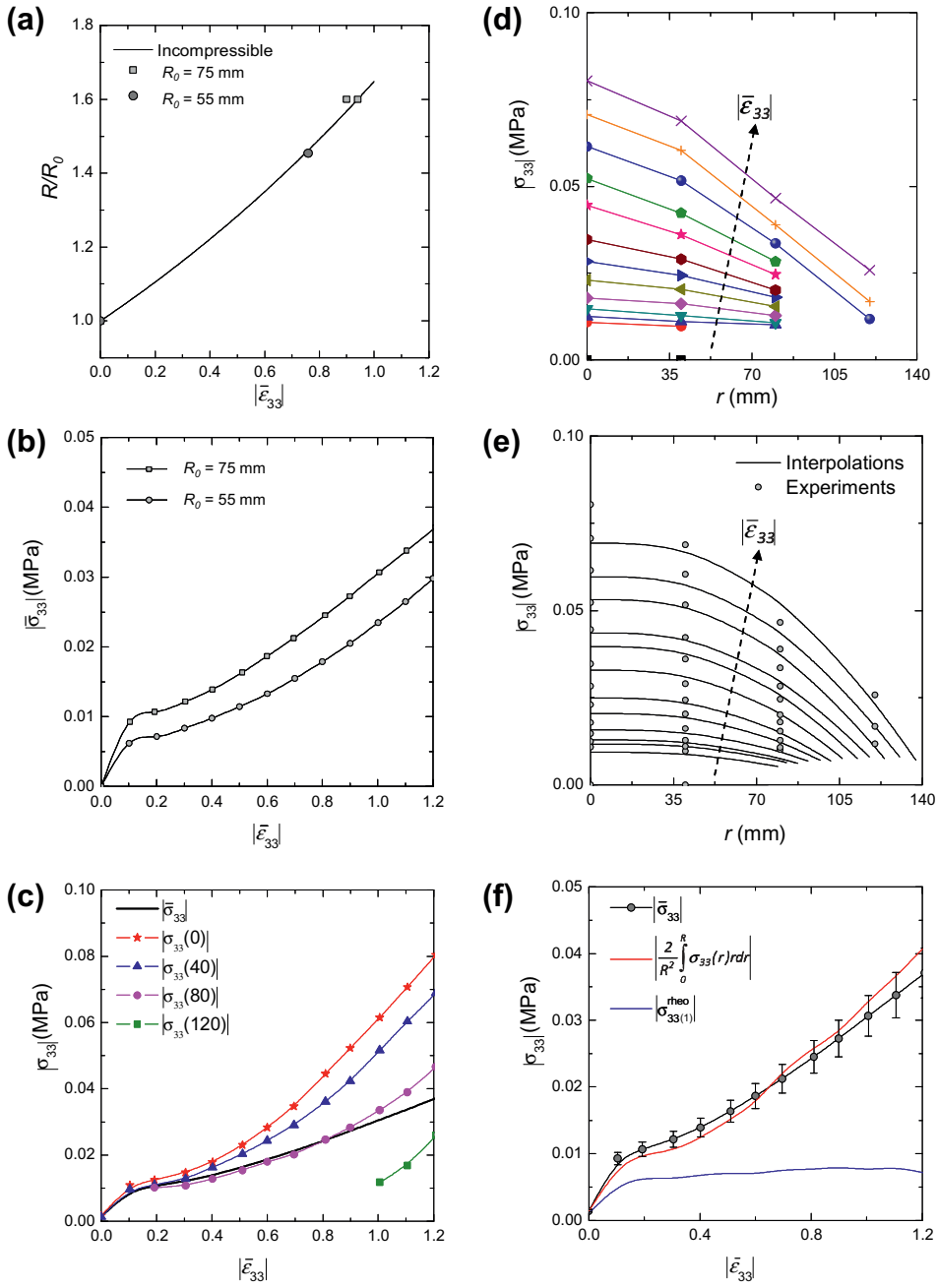

Fig. 5. Compression of the modelling plastic paste (T = 20°C). (a) Evolution of the ratio R/R_0 with respect to the average axial strain $|\bar{\varepsilon}_{33}|$ for two compressed specimens having two different diameters. (b) Evolution of the Cauchy compression stress $|\bar{\sigma}_{33}| = |F_3|h/\left(\pi h_0 R_0^2\right)$ with respect to the average axial strain $|\bar{\varepsilon}_{33}|$ for two compressed specimens having two different diameters. (c) Evolution of the local axial stresses $|\sigma_{33}(0)|$, $|\sigma_{33}(40)|$, $|\sigma_{33}(80)|$ and $|\sigma_{33}(120)|$ and of the average axial stress $|\bar{\sigma}_{33}|$ with respect to the average axial strain $|\bar{\varepsilon}_{33}|$. Experimental points (d) and interpolations (e) of the profiles of the local axial stresses measured along a radius r of the instrumented simple compression rheometer. (f) Evolution of the measured average axial stress $|\bar{\sigma}_{33}|$, the calculated intrinsic rheological stress $|\sigma^{rheo}_{33(1)}|$ and the integral from 0 to R for all axial strains of the profiles of measured local axial stresses $|\sigma_{33}(r)|$ as a function of the average axial strain $|\bar{\varepsilon}_{33}|$. (For interpretation of the references to colour in this figure legend, the reader is referred to the web version of this article.)

In a cylindrical coordinate frame $(\mathbf{e}_r, \mathbf{e}_\theta, \mathbf{e}_3)$, considering the hypothesis of the strain homogeneity and the assumption of transverse isotropy in the $(\mathbf{e}_r, \mathbf{e}_\theta)$ plane of the material, by deriving with respect to the spatial coordinates the mass balance equation and then integrating, it is easy to show that the solution of the velocity field writes:

$$\mathbf{v} = \frac{\dot{R}}{R} r\mathbf{e}_r + \frac{\dot{h}}{h} x_3 \mathbf{e}_3, \tag{2}$$

noting $v_r(r = R) = \dot{R}$ and $v_3(x_3 = h) = \dot{h}$.

Then, $\dot{\varepsilon}_v$ explicitly writes:

$$\dot{\varepsilon}_v = 2\frac{\dot{R}}{R} + \frac{\dot{h}}{h}. \tag{3}$$

5.2. Momentum balance equation

Assuming quasi-static flows and negligible volume forces, the first momentum balance equation can be written as

$$\mathbf{div}\boldsymbol{\sigma} = \mathbf{0}, \tag{4}$$

where $\boldsymbol{\sigma}$ is the Cauchy stress tensor. In order to constrain the shear components $D_{\beta 3}$ (for $\beta \in \{r,\theta\}$) of the strain rate tensor $\mathbf{D}$ to be equal to zero and consequently to ensure a simple compression kinematics, a Lagrange multiplier T is added to the expression of the stress tensor $\boldsymbol{\sigma}$ [28]. Similarly, the homogeneity of the compressibility of the composite, as expressed in Eq. (1), is obtained by adding an arbitrary pressure q to the stress tensor:

$$\boldsymbol{\sigma} = -q\delta + T(\mathbf{e}_r \otimes \mathbf{e}_3 + \mathbf{e}_3 \otimes \mathbf{e}_r) + \boldsymbol{\sigma}^e, \tag{5}$$

where $\boldsymbol{\delta}$ is the identity tensor and $\boldsymbol{\sigma}^e$ is the effective stress tensor, *i.e.* the stress that would be induced by the flow of the composite under unconstrained uniaxial compression. Taking the previous assumptions into account, the momentum balance equation in the $(\mathbf{e}_r, \mathbf{e}_\theta)$ plane, once integrated over the thickness h of the specimen and by assuming that the friction forces exerted at the interface with the upper ($x_3 = h/2$) and lower platens ($x_3 = -h/2$) are equal, now reads:

$$-\widetilde{\mathbf{grad}}Q + \frac{2}{h}\mathbf{T} + \widetilde{\mathbf{div}}\boldsymbol{\Sigma}^e = \tilde{\mathbf{0}}, \tag{6}$$

where

$$Q = \frac{1}{h}\int_{-h/2}^{h/2} q\,dx_3, \quad \boldsymbol{\Sigma}^e = \frac{1}{h}\int_{-h/2}^{h/2} \boldsymbol{\sigma}^e dx_3, \tag{7}$$

where the symbol "~" is introduced to distinguish 2D differential operators in the $(\mathbf{e}_r, \mathbf{e}_\theta)$ plane from their 3D counterparts and where, assuming that $T(x_3 = h/2) = -T(x_3 = -h/2)$:

$$(2\mathbf{T}).\mathbf{e}_r = [T]_{-h/2}^{h/2} = 2T \quad \text{and} \quad (2\mathbf{T}).\mathbf{e}_\theta = 0. \tag{8}$$

Q and $\boldsymbol{\Sigma}^e$ represent the pressure and the effective stress in the $(\mathbf{e}_r, \mathbf{e}_\theta)$ plane averaged over the thickness of the specimen, respectively. $\mathbf{T}$ is the friction tangential stress vector the specimen is subjected to at the interfaces with the rheometer. Considering the plug flow assumptions and the spatial invariance of the effective stress tensor ($\forall \mathbf{x}$, $\boldsymbol{\Sigma}^e$it has constant components), Eq. (6) along $\mathbf{e}_r$ is reduced to:

$$-Q_{,r} + \frac{2T}{h} = 0. \tag{9}$$

Then, after integration using the following boundary condition in $r = R$: $\Sigma_{rr} = -Q(R) + \Sigma_{rr}^e = 0$, the solution $Q(r)$ of Eq. (6) is expressed as

$$Q(r) = \Sigma_{rr}^e - \frac{2}{h}\int_r^R T(r')dr'. \tag{10}$$

Using the expression Eq. (5) of the stress tensor $\boldsymbol{\sigma}$ averaged over the thickness h of the specimen, one obtains:

$$\Sigma_{33}(r) = -Q(r) + \Sigma_{33}^e, \tag{11}$$

so that, using Eq. (10):

$$\Sigma_{33}(r) = \underbrace{\Sigma_{33}^e - \Sigma_{rr}^e}_{\sigma_{33}^{rheo}} + \underbrace{\frac{2}{h}\int_r^R T(r')dr'}_{\Sigma_{33}^{fric}(r)}, \tag{12}$$

where σ_{33}^{rheo} represents the intrinsic rheological behaviour of the tested material and where $\Sigma_{33}^{fric}(r)$ is the part of the axial stress due to the friction phenomena (in $r = R$, $\Sigma_{33}^{fric}(R) = 0$). This is illustrated in Fig. 4.

So far, analyses developed following the previous framework postulated several various simple analytical forms for the friction law they incorporated. Coulombic, linear or nonlinear hydrodynamic friction laws [29,15] were considered. The previously developed approaches also postulated the incompressibility of the composite ($\dot{\varepsilon}_v = 0$). Such approaches had the advantage to allow a quick estimation of the rheological properties of the tested material using Eq. (12). Unfortunately, these estimations were dependent on the nature of the *a priori* chosen friction law. Here such former approaches are completed. With the newly developed model, no *a priori* form is required for the friction law, and both incompressible and compressible flows can be treated. The developed model relies on the use of the derivative form of Eq. (11) with respect to r and the first equation of the system (9):

$$T = -\frac{h}{2}\frac{\partial \Sigma_{33}(r)}{\partial r}. \tag{13}$$

To our knowledge, this expression is new. It shows that once the profile of $\Sigma_{33}(r)$ is known (this is the case when using the newly developed rheometer and its normal stress sensors), it is possible to determine experimentally the friction law T without *a priori* assumptions about the incompressibility and the form of the rheological behaviour law of the composite. In the case of specimens having a small thickness h (like in this work) the gradient of σ_{33} along $\mathbf{e}_3$ can be considered as weak enough [29], so that $\Sigma_{33} \approx \sigma_{33}$. The friction law can thus be obtained for each mould–composite interface point by using the profiles of the measured local axial stresses $\sigma_{33}(r)$ and their derivatives with respect to r. Besides, it is possible to calculate the average axial stress $\bar{\sigma}_{33}$:

$$\bar{\sigma}_{33} = \frac{F_3}{\pi R^2} = -\frac{2}{R^2}\int_0^R q(r,x_3)rdr + \sigma_{33}^e, \quad \forall x_3. \tag{14}$$

In particular, it can also be written in $x_3 = h/2$, *i.e.* on the upper surface of the specimen. It is then possible to show [28] that

$$\int_0^R Q(r)rdr = \int_0^R q(r, x_3 = h/2)rdr. \tag{15}$$

The average axial stress $\bar{\sigma}_{33}$ may also be seen as the sum of a friction contribution of the composite with the compression platens $\bar{\sigma}_{33}^{fric}$ and a rheological contribution σ_{33}^{rheo}:

$$\bar{\sigma}_{33} = \underbrace{\sigma_{33}^e - \sigma_{rr}^e}_{\sigma_{33}^{rheo}} + \underbrace{\frac{4}{hR^2}\int_0^R \left(\int_r^R T(r')dr'\right)rdr}_{\bar{\sigma}_{33}^{fric}}. \tag{16}$$

Without friction, note that all local axial stresses $\sigma_{33}(r)$, $\forall r \in [0,R]$, are equal to the average axial stress $\bar{\sigma}_{33}$.

Thus, during compression tests, the newly developed rheometer gives the local axial stresses $\sigma_{33}(r)$ measured in $r = 0$, 40, 80, 120 and 160 mm. Then, it is possible to interpolate the profiles of local axial stresses during the compression of the specimens. The fitted functions can be used to extrapolate $\sigma_{33}(r = R)$ and to obtain the rheological behaviour of the tested material. This method necessitates to know the current radius R of the specimens that can be calculated when the local axial stress sensors detect the flow front progression. The stress profiles can then be derived as presented above to obtain the friction law T. Furthermore, it is possible to calculate the average axial stress $\bar{\sigma}_{33}$ with the measurements of F_3.

6. Validation of the methodology

In order to validate the above methodology lubricated simple compression tests were first performed using the modelling plastic paste (see Section 2). The recorded scatter of the data remained about ±10%. It was checked that the plug flow assumption was correct in all testing conditions.

6.1. Incompressibility of the modelling plastic paste

The local axial stress sensors allowed the evolution of the radius of tested samples to be followed during these tests, see

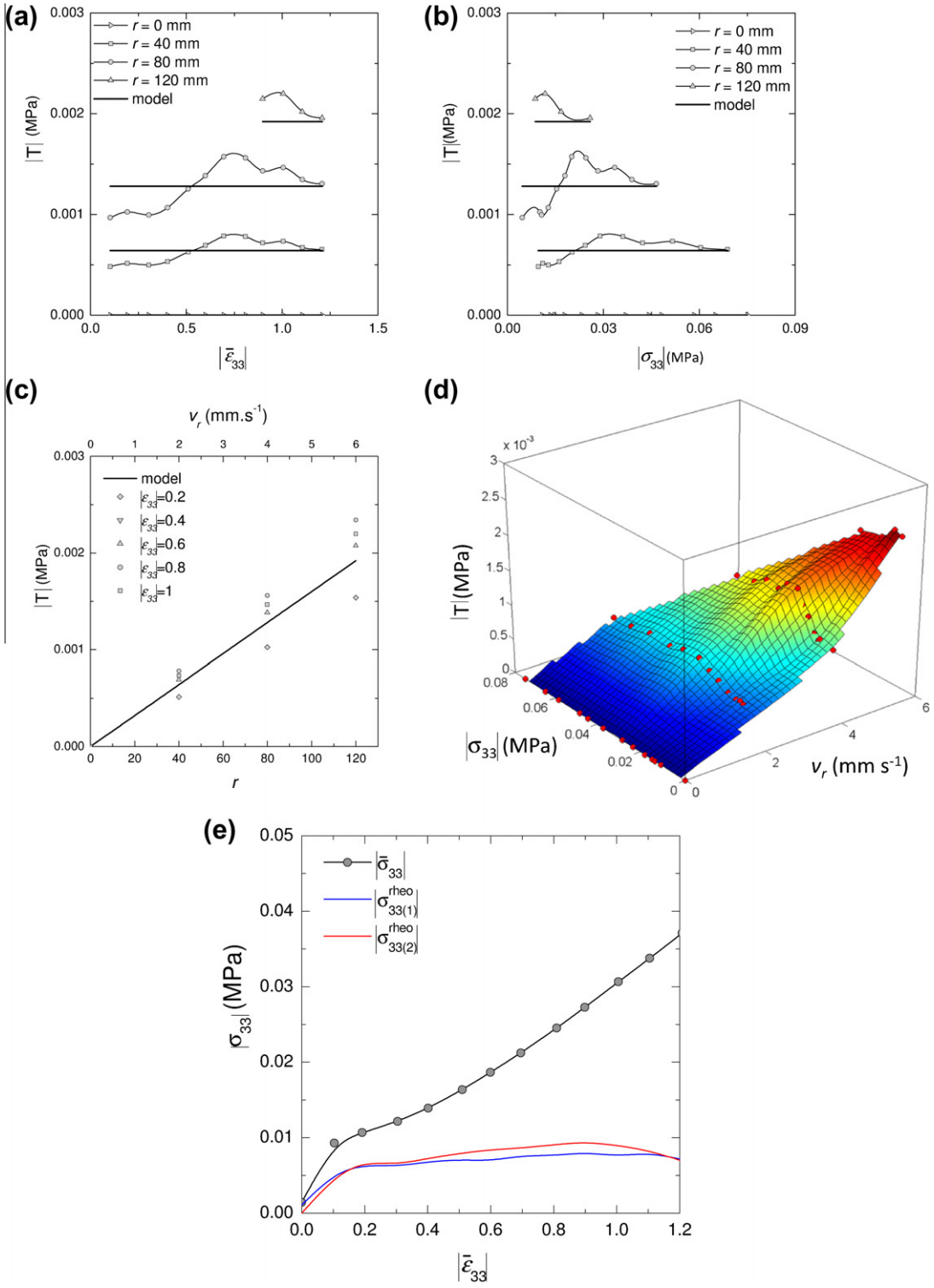

Fig. 6. Compression of the modelling plastic paste (T = 20 °C). (a) Evolution of $|T|$ with respect to the average axial strain $|\bar{\varepsilon}_{33}|$ for various positions, r = 0, 40, 80, 120 mm, of the local stress sensors. (b) Evolution of $|T|$ with respect to the local axial stress $|\sigma_{33}|$ for various radii r = 0, 40, 80, 120 mm. (c) Evolution of $|T|$ with respect to the radius r for various average axial strains $|\bar{\varepsilon}_{33}| = 0$, 0.2, 0.4, 0.6, 0.8, 1 and 1.2. (d) Friction law as a function of the paste velocity v_r and of the local axial stress $|\sigma_{33}|$. (e) Comparison of the rheological behaviour of the modelling plastic paste obtained using three different methods. (For interpretation of the references to colour in this figure legend, the reader is referred to the web version of this article.)

Fig. 5a. Comparing the experimental points with the theoretical curves, drawn in the case of incompressibility shows that the modelling plastic paste can be considered as incompressible.

6.2. Evidence of friction effects at the mould–paste interface

In Fig. 5b, the evolution of the average axial stresses $\bar{\sigma}_{33} = F_3 h / \left(\pi h_0 R_0^2\right)$ (estimated considering the incompressibility)

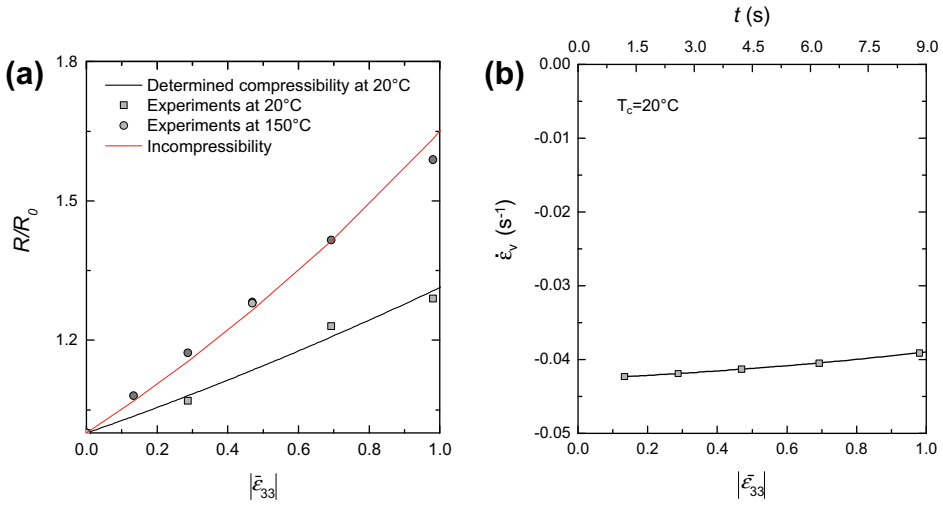

Fig. 7. Compression of SMC performed without lubrication. (a) Evolution of the ratio R/R_0 of the specimens as a function of the average axial strain $|\bar{\varepsilon}_{33}|$ for two temperatures of 20 °C and 150 °C. (b) Evolution of the surface change rate with $|\bar{\varepsilon}_{33}|$. (For interpretation of the references to colour in this figure legend, the reader is referred to the web version of this article.)

with respect to the average axial strain $\bar{\varepsilon}_{33}$ is depicted for samples which have two various initial radii R_0. It can be observed that the measured average axial stress is lower for samples having an initial radius $R_0 = 55$ mm than for specimens having an initial radius of 75 mm. Furthermore, the evolution of local axial stresses with the average axial strain $\bar{\varepsilon}_{33}$ are compared to that of the average axial stress $\bar{\sigma}_{33}$ in Fig. 5c. This figure collects the results of 15 identical tests and shows that the local axial stresses measured in $r = 0$, 40 and 80 mm are higher than the average axial stress $\bar{\sigma}_{33}$ throughout the deformation. Within the previously presented theoretical framework, these two observations can be interpreted as the occurrence of non-negligible friction effects at the mould–material interface.

6.3. Determination of the rheological behaviour of the modelling plastic paste

Fig. 5d shows the profiles of the local axial stresses as a function of the radius r for a wide range of compression strain $\bar{\varepsilon}_{33}$ up to a maximum equal to 1.2. The chosen fitting function for these profiles are quadratic:

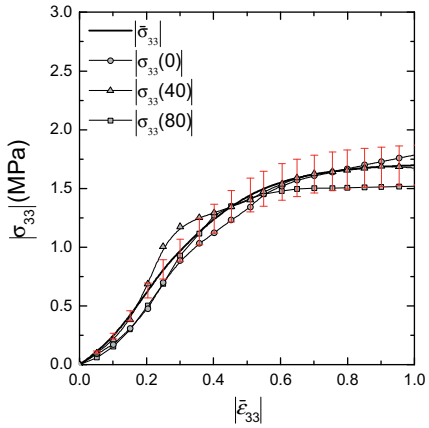

Fig. 8. Compression tests of SMC performed with lubrication ($T = 20$ °C): evidence of no friction effects. Evolution of the average axial stress $|\bar{\sigma}_{33}|$ and the local axial stresses $|\sigma_{33}(r)|$ measured in $r = 0$, 40 and 80 mm as a function of the average axial strain $|\bar{\varepsilon}_{33}|$. (For interpretation of the references to colour in this figure legend, the reader is referred to the web version of this article.)

$$\sigma_{33}(r) = Ar^2 + Br + C. \tag{17}$$

These functions are drawn in Fig. 5e for each average axial strain $\bar{\varepsilon}_{33}$ with $C \approx \sigma_{33}(0)$, which is given from the test data. Besides, the symmetry of the test induces that $B = \frac{\partial \sigma_{33}}{\partial r}(0) = 0$. The parameter A can be determined from the constraint imposed by Eq. (14): see the second member of this equation where $R = \sqrt{h_0/h}R_0$ is obtained from the incompressibility of the modelling plastic paste. Using the interpolated profiles of local axial stresses $\sigma_{33}(r)$, the rheological behaviour of the tested material $\sigma^{rheo}_{33(1)}$ can thus be obtained, *e.g.* in $r = R$:

$$\sigma_{33}(R) = \sigma^{rheo}_{33(1)} = AR_0^2\frac{h_0}{h} + C. \tag{18}$$

On the one hand, it appears in Fig. 5f that the fitted local stresses $\sigma_{33}(r)$, once integrated from 0 to R, are very close to the average axial stress $\bar{\sigma}_{33}$ measured with the press load cell: the chosen fit is then correct to satisfy this constraint. On the other hand, it can be observed that the rheology of the modelling plastic paste $\sigma^{rheo}_{33(1)}$ is largely different from the measured average axial stress $\bar{\sigma}_{33}$, *i.e.* with F_3: this highlights that it is very important to properly correct the raw acquired data.

6.4. Analysis of friction phenomena

The friction law T can be obtained when deriving the profiles of the local axial stresses with respect to r. From Eq. (13), assuming that the quadratic fitting functions are satisfactory:

$$T = -Arh. \tag{19}$$

Fig. 6a and b shows respectively the variations of T with respect to the average axial strain $\bar{\varepsilon}_{33}$ and the local axial stress σ_{33}. A slight increase of T can be noticed up to an average axial strain $\bar{\varepsilon}_{33} \approx -0.6$, which corresponds to a local axial stress $\sigma_{33} \approx -0.02$ MPa. This might be due to the lubrication layer which might be (partially) expelled at the beginning of the test. Then, T tends to stabilize. This effect might be related to a remaining lubrication layer of uniform thickness between the rheometer platens and the specimen. Fig. 6c shows that the increasing variation of T with the paste radial velocity $v_r = -r\bar{D}_{33}/2$ can be considered as linear. Using the previous expression for the paste velocity v_r and the expression (19) of T, it is possible to write:

$$T = -Ahr = \frac{2Ah}{\overline{D}_{33}} v_r, \tag{20}$$

which highlights the pronounced hydrodynamic nature of friction phenomena occurring during these tests. Fig. 6d gives a summary of the previous graphs and displays the variation of T with respect to σ_{33} and v_r. This graph illustrates the complexity of the friction phenomena. These results could be further used to *a posteriori* propose friction laws. For instance, if the product Ah in the previous equation is considered as being not dependent on the strain, a hydrodynamic and linear friction law can be proposed [29,27,28]. An average hydrodynamic coefficient $\lambda \approx -\frac{2\langle Ah\rangle}{\overline{D}_{33}} \approx 3.2\times 10^{-4}$ N s mm^{-3} can then be defined, where $\langle Ah\rangle$ is the average value of Ah over the whole deformation. Thus, a model for the friction law can be written as follows:

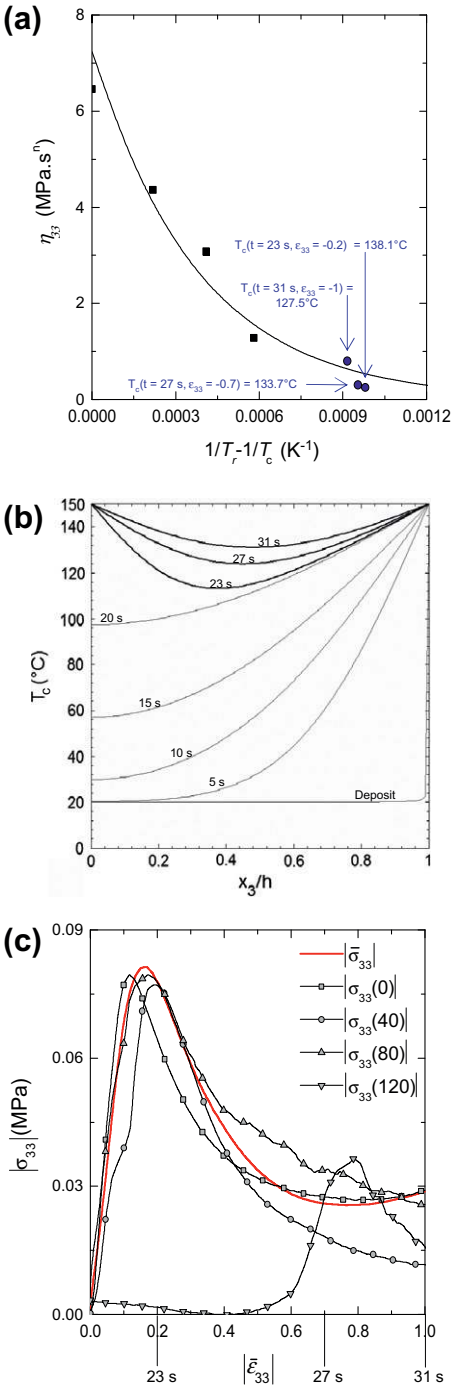

Fig. 9. (a) Evolution of the compression viscosity η_{33} of SMC at $|D_{33}| = 1$ s^{-1} with the following expression $\frac{1}{T_r} - \frac{1}{T_c}$ where T_c is the current temperature and $T_r = 296$ K a reference temperature. (b) Temperature profiles through the thickness of the SMC specimen (grey lines indicate the deposit period, whereas black lines indicate the compression period). (c) Evolution of the average axial stress $|\bar{\sigma}_{33}|$, the local axial stresses $|\sigma_{33}(r)|$ measured in $r = 0$, 40, 80 and 120 mm as a function of the average axial strain $|\bar{\varepsilon}_{33}|$ during anisothermal compression at 150 °C without lubrication. (For interpretation of the references to colour in this figure legend, the reader is referred to the web version of this article.)

It is possible to check the model validity using the compression data and the second member of Eq. (12). From the expression of T^{mod}, $\Sigma_{33}^{fric}(r)$ reads:

$$\Sigma_{33}^{fric}(r) = \frac{\lambda \overline{D}_{33}}{2h}(R^2 - r^2), \tag{22}$$

which allows the rheological response of the modelling plastic paste response $\sigma_{33(2)}^{rheo}$ to be calculated considering Eq. (12) and the data of the local stress sensor, in $r = 0$, for instance. In Fig. 6e, $\sigma_{33(2)}^{rheo}$ is plotted with respect to the axial strain $\bar{\varepsilon}_{33}$. It is obvious that the rheological response estimated when using the model friction law, $\sigma_{33(2)}^{rheo}$, can be well compared with the estimation $\sigma_{33(1)}^{rheo}$ based on the fitting of the local axial stresses. Thus, a simple hydrodynamic friction model could be sufficient in this particular case.

7. Application to an industrial SMC

The results of a series of compression tests achieved with the previously described SMC are given in this section. Most of the tests were performed in isothermal conditions at 20 °C, using lubrication or not. Note that other lubricated compression tests were performed at 40 °C, 60 °C and 80 °C. Furthermore, some tests were also carried out in anisothermal conditions at a temperature of 150 °C without lubrication in order to mimic industrial forming conditions. Note that the experimental procedure was slightly different at low testing temperatures (20–80 °C) and at the highest testing temperature of 150 °C. At low temperatures, tests were preceded by a preliminary stage where the specimens were pre-compressed (0.5 mm) in order to flatten the initial wavy surfaces of SMC charges. At this stage, the initial specimen thickness h_0 was measured. Compression tests started once the pre-compression force was completely relaxed. At 150 °C, to mimic the industrial compression moulding conditions, the following procedure was adopted: once the specimens were put in contact with the lower platen of the rheometer, the compression test was launched. After 20 s the upper platen reached the specimen surface, then the compression continued and the initial thickness of the specimen was arbitrarily defined and measured once the compression stress reached approximately 5.7×10^{-3} MPa. This pre-compaction corresponds approximately to the same height reduction (≈0.5 mm) as in the case of tests performed at 20 °C.

7.1. SMC compressibility at 20 °C and 150 °C

Fig. 7a shows the evolution of the ratio R/R_0 of tested SMC specimens as a function of the average axial strain at both temperatures of 20 °C or 150 °C. At the lowest temperature, the SMC can be clearly seen as a compressible material, since $\dot{\varepsilon}_v < 0$, see Fig. 7b. At 150 °C, the situation is different as the SMC specimens appear to be incompressible: $\dot{\varepsilon}_v \approx 0$. At 20 °C, the observed mechanisms can be related to a progressive decrease of the porosity of SMC.

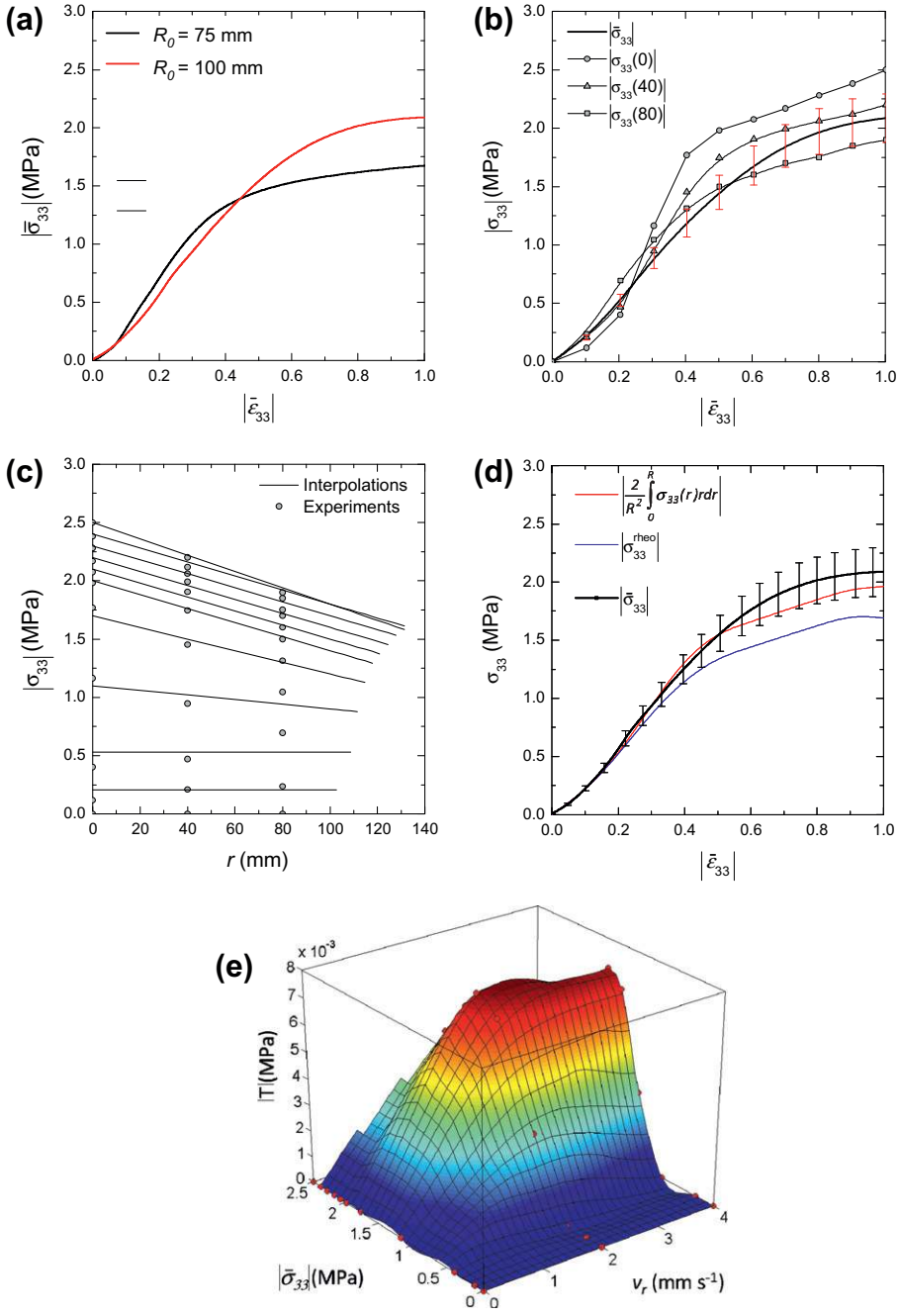

Fig. 10. Compression of SMC without lubrication (T = 20°C). (a) Evidence of friction phenomena: evolution of the average axial stress $|\bar{\sigma}_{33}|$ as a function of the average axial strain $|\bar{\varepsilon}_{33}|$ for two specimens having different initial diameters. (b) Evidence of mould–composite friction phenomena from the local axial stress measurements. (c) Profiles of the local axial stresses $|\sigma_{33}(r)|$ along the radius r: experimental points and interpolations. (d) Evolution of the measured average axial stress $|\bar{\sigma}_{33}|$, the calculated intrinsic rheological stress $|\sigma_{33}^{rheo}|$, the integral from 0 to R for all strains of the measured local axial stresses $|\sigma_{33}(r)|$ as a function of the average axial strain $|\bar{\varepsilon}_{33}|$. (e) Friction law $|T|$ as a function of the velocity v_r and the local axial stress $|\sigma_{33}|$ of the composite. (For interpretation of the references to colour in this figure legend, the reader is referred to the web version of this article.)

Yet, at this stage of investigation, it cannot be concluded about the mechanisms which govern the observations made in Fig. 7 for the temperature of 150 °C. Does the stage preceding in this case the measurement of the initial thickness remove the porosity of the SMC which becomes denser and as a result incompressible? Do the pores remain even after this first stage? Are these latter transported during flow? This point should be clarified in further study by performing *in situ* observations, for instance. Nonetheless, these observations highlight the large differences the SMC compounds exhibit for various thermomechanical loading conditions.

7.2. SMC rheology and friction phenomena at 20 °C, 40 °C, 60 °C, and 80 °C, tests with lubrication

Fig. 8 depicts the SMC rheological response measured at 20 °C during compression tests with lubrication. Whatever the considered axial strain, it appears that the local axial stresses $\sigma_{33}(r)$ measured in r = 0, 40 and 80 mm are equal to the average axial stress $\bar{\sigma}_{33} = F_3/(\pi R^2)$ (for the estimation of R: see the fitted line given in Fig. 7). In this situation, the contribution of the friction effects is obviously negligible and the data thus

correspond to the intrinsic rheological behaviour of SMC. For the temperatures of 40 °C, 60 °C, and 80 °C, the experimental observations are similar to those made at 20 °C. In addition, the continuous line drawn in Graph (a) of Fig. 9 depicts the SMC compression viscosity $\eta_{33} = \bar{\sigma}_{33}/D_{33}$ as a function of $\frac{1}{T_r} - \frac{1}{T_c}$, where T_c is the current temperature and $T_r = 296$ K is a reference temperature. The continuous line represents an Arrhenius law $\eta_{33}(T_c) = \eta_{33}(T_r)\exp\left(b\left(\frac{1}{T_r} - \frac{1}{T_c}\right)\right)$ fitted for temperatures ranging between 20 °C and 80 °C ($b = 2600\ \mathrm{K}^{-1}$).

7.3. SMC rheology and friction phenomena at 20 °C, tests without lubrication

Friction effects already observed in this situation in Fig. 3 (or Fig. 10 where the Cauchy stress is used) are confirmed in Fig. 10b which shows the measurements of the local axial stress sensors using samples having an initial radius $R_0 = 100$ mm. For instance, the local axial stresses measured in $r = 0$ and 40 mm are larger than the average axial stress $\bar{\sigma}_{33}$. This friction influence is also highlighted in Fig. 10c where it can be observed that the local stress profiles decrease with the specimens' radius. The SMC rheological behaviour and the friction law were identified following the method described for the modelling plastic paste. Fig. 10c depicts the local stress profiles fitted here with linear functions with r:

$$\begin{cases} \sigma_{33}(r) = Ar + B \quad \forall r \in]0, R] \\ \sigma_{33}(r) = B \quad \text{in } r = 0 \end{cases} \tag{23}$$

As for the modelling paste, it should be noticed that the chosen interpolation for $\sigma_{33}(r)$, once integrated from 0 to R, allows the average axial stress $\bar{\sigma}_{33}$ to be reasonably estimated: see Fig. 10d. This method also gives the intrinsic rheological behaviour $\sigma_{33}^{rheo} = \sigma_{33}(R)$ of the tested SMC where the evolution of the sample radius R (see Fig. 10) and $B = \sigma_{33}(0)$ are experimentally determined. The as-determined evolution of σ_{33}^{rheo} with the axial strain is illustrated in Fig. 10d. It appears that its value can be up to approx. 25% lower (at $\bar{\varepsilon}_{33} = -0.8$) than the average axial stress $\bar{\sigma}_{33}$. Again, this illustrates that a large error can be made if the friction contribution is not accounted for during the data analysis. In order to further validate the employed analysis method, the as-determined curve for the SMC intrinsic rheological behaviour is now compared in Fig. 11 with the similar curve obtained from the tests performed with very good lubrication conditions (see Fig. 8): the two curves are nearly superimposed. Finally, the friction law is determined:

$$T = -Ah/2. \tag{24}$$

Its experimental evolution with respect to $\bar{\sigma}_{33}$ and v_r is given in Fig. 10e where it is obvious that the mould–SMC friction law exhibited is largely different from that determined for the modelling plastic paste.

7.4. Anisothermal tests at 150 °C without lubrication

In Fig. 9c, the rheological behaviour measured during anisothermal compression tests at 150 °C without lubrication is radically different from that observed for 20 °C tests. The average axial stress $\bar{\sigma}_{33}$ indeed increases up to an axial strain $\bar{\varepsilon}_{33} = -0.2$, then decreases up to an axial strain $\bar{\varepsilon}_{33} = -0.7$. Over this value of strain, the axial stress seems to slightly increase again. In Fig. 9c, the local axial stresses $\sigma_{33}(r)$ can be considered as being more or less equal to the average axial stress $\bar{\sigma}_{33}$ whatever the radius r or the axial strain $\bar{\varepsilon}_{33}$. During these compression tests at "high" temperature, it was difficult to clearly appreciate the SMC flow mechanisms as the marks drawn onto the surface of the specimens tended to vanish. As some marks drawn on the perimeter of the specimens could be observed on the outer radius of the compressed specimens, it was considered that the flow conditions were quite homogeneous and corresponded to a plug flow. These observations show that the friction effects during such flow at high temperature can be neglected. This remark is valid for this particular couple "SMC plus aluminium compression platens", but is opposite to the observations made by Dumont et *al.* [28] for a SMC flowing inside a chrome-plated steel mould, for instance.

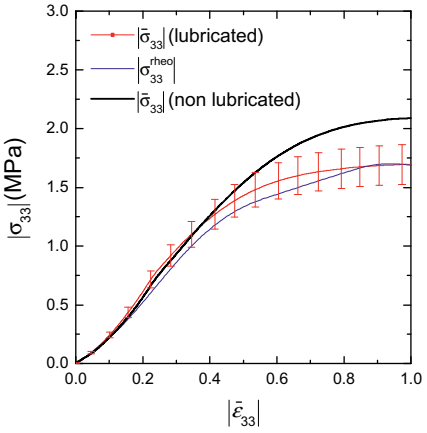

Fig. 11. Compression of SMC ($T = 20$ °C). Comparison of the corrected average axial stress (obtained when performing non-lubricated tests), the measured axial stress during non-lubricated tests (phenomena of friction are occurring) and the average axial stress obtained from lubricated tests (no friction effects). (For interpretation of the references to colour in this figure legend, the reader is referred to the web version of this article.)

The overall decrease of the stress measured during compression tests may be attributed to the increasing temperature inside the SMC charge. This latter was estimated at various times: between 0 and 20 s, *i.e.* the deposit period of the SMC charge in the mould cavity up to the contact time with the upper platen, at 23 s, 27 s and 31 s after deposition, *i.e.* during the compression phase for $\bar{\varepsilon}_{33} = -0.2$, -0.7 and -1, respectively, following for that the heat conduction model proposed by Barone and Caulk [29], considering perfect mould–SMC thermal contact and the charge deformation during compression. Eq. (6.1) proposed by Barone and Caulk [29] was used for simulating the temperature increase during deposit, whereas Eq. (6.6) of the same study was solved to estimate the temperature profiles through the thickness of the SMC charge during the processing phase. Also note that the thermal parameters proposed in this former study were used. Simulated temperature profiles are given in Fig. 9b. If after 20 s, the temperature profile is asymmetric through the charge thickness, at 23 s, 27 s and 31 s it becomes largely narrower. Consequently, the SMC compression viscosity $\eta_{33} = \bar{\sigma}_{33}/\overline{D}_{33}$ was roughly estimated considering the through-thickness averaged temperatures for these various times: see the points shown by an arrow in Fig. 9a. It appears that the experimental points and the previously extrapolated Arrhenius law remain close, which would confirm that it is possible to roughly identify such a rheological parameter when using an anisothermal and non-lubricated compression rheometry method.

8. Conclusion

Due to their processing route, polymer composites such as SMC, GMT, and CMT are porous materials when being compression moulded. The influence of such porosity has a potential influence on the compressibility of such materials during compression. The vast majority of experimental and modelling approaches neglect this aspect of the flow behaviour, but it must be investigated. For example, the unique industrial formulation of SMC tested in this

study indeed reveals that such material can be very compressible or incompressible depending on the testing conditions. This study also revealed that the analysis of simple compression tests and consequently the determination of rheological parameters can be distorted due to large errors that arise from friction effects occurring at the mould–composite interface. The friction effects observed during such rheometry experiments are similar from a phenomenological point of view to those observed during industrial compression mouldings that are induced by the shearing of a thin layer of polymeric paste in the case of industrial compounds.

Therefore a new rheometer was designed to analyse both phenomena. This apparatus is equipped with sensors to measure *in situ* the normal local stress along the radius of one compression platen. Coupled to this rheometer, an analysis method of the acquired data was proposed to determine the compressibility of the studied composite and the friction forces arising at the mould–composite interface. It was shown that friction forces could be estimated without making any *a priori* assumptions on their nature. The use of this new apparatus and of the associated analysis method were proven to be successful to characterise the rheological behaviour and the friction behaviour of several materials like a modelling plastic paste and an industrial SMC for various lubrication conditions and temperatures ranging from 20 °C to 150 °C, *i.e.* conditions close to an industrial moulding. This preliminary work has to be further pursued to better understand the tribology of the mould–composite interface.

Acknowledgements

This work was performed within the Research Project "MOC" of the competitiveness cluster Plastipolis and the ESRF Project "Real Time Microtomography dedicated to the *in situ* rheology of fibre-reinforced polymer composites during their forming process" (exp. MA-878). Mixt Composites Recyclables (A. Tourbez) is gratefully acknowledged for supplying SMC materials. O. Guiraud would like to thank the Région Rhône-Alpes (France) and the competitiveness cluster Plastipolis (France) for his research grant.

References

[1] Orgéas L, Dumont PJJ. Sheet molding compounds. In: Nicolais L, Borzacchiello A, Lee SM, editors. Wiley Encyclopedia of Composites, 2nd ed., Wiley; 2012. p. 2683–718. ISBN: 978-0-470-12828-2.
[2] Boyard N, Millischer A, Sobotka V, Bailleul J-L, Delaunay D. Behaviour of a moulded composite part: modelling of dilatometric curve (constant pressure) or pressure (constant volume) with temperature and conversion degree gradients. Compos Sci Technol 2007;67:943–54.
[3] Törnqvist R, Sunderland P, Månson J-AE. Non-isothermal process rheology of thermoplastic composites for compression flow moulding. Composites: Part A 2000;31:917–27.
[4] Wakeman MD, Rudd CD. Compression molding of thermoplastic composites. In: Kelly A, Zweben C, editors. Comprehensive composite materials, vol. 2. Elsevier; 2000. p. 915–63. ISBN: 0-080437206.
[5] Orgéas L, Dumont PJJ, Michaud V, Favier D. Separation of the polymer matrix and the fibrous reinforcement during compression moulding of Glass Mat Thermoplastics (GMT). Int J Mater Form 2008;1:929–32.
[6] Caba AC, Loos AC, Batra RC. Fibre–fibre interactions in carbon mat thermoplastics. Composites: Part A 2007;38:469–83.
[7] Feraboli P, Peitso E, Cleveland T, Stickler PB, Halpin JC. Notched behavior of prepreg-based discontinuous carbon fiber/epoxy systems. Composites: Part A 2009;40:289–99.
[8] Feraboli P, Cleveland T, Ciccu M, Stickler P, DeOto L. Defect and damage analysis of advanced discontinuous carbon/epoxy composite materials. Composites: Part A 2010;41:888–901.
[9] Barone MR, Caulk DA. Kinematics of flow of sheet molding compounds. Polym Compos 1985;6:105–9.
[10] Odenberger P, Andersson H, Lundström T. Experimental flow-front visualisation in compression moulding of SMC. Composites: Part A 2004;35:1125–34.
[11] Chalencon F, Orgéas L, Dumont PJJ, Foray G, Cavaillé J-Y, Maire E, et al. Lubricated compression and X-ray microtomography to analyse the rheology of a fibre-reinforced mortar. Rheol Acta 2010;49:221–35.
[12] Charalambides MN, Goh SM, Lim L, Williams JG. The analysis of the frictional effect on stress–strain data from uniaxial compression of cheese. J Mater Sci 2001;36. 2321-2321.
[13] Charalambides MN, Goh SM, Wanigasooriya L, Williams JG, Xia W. Effect of friction on uniaxial compression of bread dough. J Mater Sci 2005;40:3375–81.
[14] Le Corre S, Orgéas L, Favier D, Tourabi A, Maazouz A, Venet C. Shear and compression behaviour of sheet molding compounds. Compos Sci Technol 2002;62(4):571–7.
[15] Dumont P, Orgéas L, Le Corre S, Favier D. Anisotropic viscous behaviour of sheet molding compounds (SMC) during compression molding. Int J Plast 2003;19:625–46.
[16] Guiraud O, Dumont PJJ, Orgéas L. How to prepare SMC and BMC-like materials to perform relevant rheological experiments? Appl Compos Mater, 2012 (online).
[17] Orgéas L, Dumont PJJ, Le T-H, Favier D. Lubricated compression of BMC, a concentrated and fibre-reinforced granular polymer suspension. Rheol Acta 2008;47:677–88.
[18] Guiraud O, Dumont PJJ, Orgéas L, Vassal J-P, Le T-H, Favier D. Towards the simulation of mould filling with polymer composites reinforced with mineral fillers and short fibres. Int J Mater Form 2010;3:S1313–26.
[19] Engmann J, Servais C, Burbidge AS. Squeeze flow theory and applications to rheometry: a review. J Non-Newtonian Fluid Mech 2005;132:1–27.
[20] Kotsikos G, Gibson AG. Rheology of glass mat thermoplastics and sheet moulding compounds. Plast Rubber Compos Process Appl 1998;27:179–84.
[21] Kotsikos G, Gibson AG. Investigation of the squeeze flow behaviour of Sheet Moulding Compounds (SMC). Composites: Part A 1998;29A:1569–77.
[22] Gibson A, Toll S. Mechanics of the squeeze flow of planar fibre suspensions. J Non-Newtonian Fluid Mech 1999;82:1–24.
[23] Estellé P, Lanos C, Perrot A, Servais C. Slipping zone location in squeeze flow. Rheol Acta 2006;45:444–8.
[24] Estellé P, Lanos C. Squeeze flow of bingham fluids under slip with friction boundary conditions. Rheol Acta 2007;46:397–404.
[25] Comte E, Merhi D, Michaud V, Månson JAE. Void formation and transport during SMC manufacturing: effect of the glass fiber sizing. Polym Compos 2006;27(3):289–98.
[26] Le T-H, Dumont P, Orgéas L, Favier D, Salvo L, Boller E. X-ray phase contrast microtomography for the analysis of the fibrous microstructure of SMC composites. Composites: Part A 2008;39:91–103.
[27] Abrams L, Castro J. Predicting molding forces during sheet molding compound (SMC) compression molding. I: Model development. Polym Compos 2003;24: 291–303.
[28] Dumont P, Orgéas L, Favier D, Pizette P, Venet C. Compression moulding of SMC: in situ experiments, modelling and simulation. Composites: Part A 2007;38:353–68.
[29] Barone MR, Caulk DA. A model for the flow of a chopped fibre reinforced polymer compound in compression molding. J Appl Mech 1986;53(191): 361–70.
[30] Barone M, Osswald T. Boundary integral equations for analyzing the flow of a chopped fiber reinforced polymer compound in compression molding. J Non-Newtonian Fluid Mech 1987;26:185–206.
[31] Osswald T, Tucker C. Compression mold filling simulation for non planar parts. Int J Polym Process 1990;5(2):79–87.
[32] Dumont P, Vassal J-P, Orgéas L, Michaud V, Favier D, Månson J-AE. A model material of highly concentrated fiber suspensions. Rheol Acta 2007;46: 639–51.